Single-Layer Materials

DOI: 10.1002/anie.201400273

Surface-Confined Single-Layer Covalent Organic Framework on Single-Layer Graphene Grown on Copper Foil**

Lirong Xu, Xin Zhou, Wei Quan Tian, Teng Gao, Yan Feng Zhang, Shengbin Lei, and Zhong Fan Liu*

Abstract: *The integration of 2D covalent organic frameworks (COFs) with atomic thickness with graphene will lead to intriguing two-dimensional materials. A surface-confined covalently bonded Schiff base network was prepared on single-layer graphene grown on copper foil and the dynamic reaction process was investigated with scanning tunneling microscopy. DFT simulations provide an understanding of the electronic structures and the interactions between the surface COF and graphene. Strong coupling between the surface COF and graphene was confirmed by the dispersive bands of the surface COF after interaction with graphene, and also by the experimental observation of tunneling condition dependent contrast of the surface COF.*

Covalent organic frameworks (COFs), in which molecular building blocks are linked by covalent bonds into two-dimensional or three-dimensional porous crystalline networks, provide robust materials that allow precise control over the composition, topology, and porosity.[1–3] 2D COFs with layered structures stacked together through van der Waals interactions are ideally suited for efficient energy storage and charge transport. However, these so-called 2D COFs differ from "true" 2D materials in the same way that graphene shows different properties from graphite. However, if isolated, a single layer of a 2D COF will satisfy in all aspects the definition of 2D polymer[4] and these periodic covalent molecular sheets with well-defined structures may provide a novel pathway to achieve control over carrier transport by quantum effects. Such 2D polymers constructed by pure organic building blocks have the promise of tuning the properties of a device through rational chemical design and synthesis.[5] The band alignment of such materials can be precisely and predictably controlled by programmable design of the starting materials.[6] Thus, in the quest for new functional materials with unprecedented properties, the preparation of "true" 2D materials has recently attracted much attention.[7,8]

The on-surface synthesis of COFs on single-crystal surfaces provides the possibility to obtain 2D polymers with single-layer thickness.[9,10] The surface could not only promote the ordering of the surface COF through epitaxial effects, but also play a role in catalysis.[10–16] Recently, long-range-ordered surface COFs based on the condensation of boronic acids, or between aldehydes and amines, were successfully synthesized under both open and closed environments with moderate heating.[14–16] However, these single-layer crystalline surface COFs are all synthesized on either metal or graphite surface, thus making them difficult to exfoliate.

A key aspect for the application of 2D polymers in nanoelectronics is to extend the polymer into a two-dimensional network through conjugation to facilitate in-plane charge transfer. Herein, we pursue a simple method to synthesize a 2D extended aromatic Schiff base surface COF with single atomic thickness on single-layer graphene grown by CVD on copper foil (SLG-copper). The formation of the framework was monitored in situ by scanning tunneling microscopy (STM) of the octanoic acid/SLG-copper interface. Benzene-1,3,5-tricarbaldehyde (BTA) and *p*-phenylenediamine (PDA) were used as precursors (Scheme 1). Though

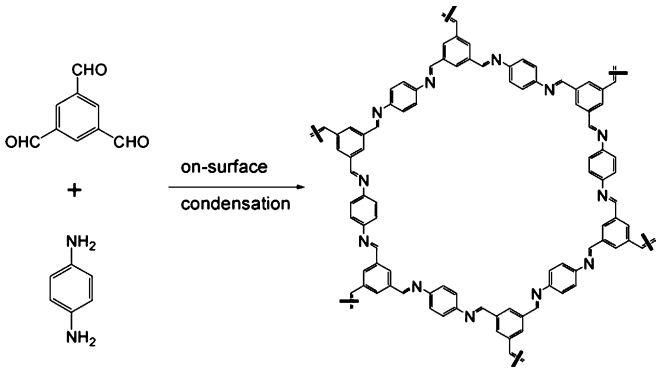

Scheme 1. Reaction scheme of benzene-1,3,5-tricarbaldehyde (BTA) and *p*-phenylenediamine (PDA) into hexagonal 2D surface $COF_{BTA\text{-}PDA}$.

[*] L. R. Xu,[+] Prof. S. B. Lei
Key Laboratory of Microsystems and Microstructures Manufacturing
Ministry of Education, Harbin Institute of Technology
Harbin, 150080 (P.R. China)
E-mail: leisb@hit.edu.cn

X. Zhou,[+] Prof. W. Q. Tian
State Key Laboratory of Urban Water Resource and Environment
Theoretical and Simulational Chemistry
Academy of Fundamental and Interdisciplinary Science
Harbin Institute of Technology
Harbin, 150080 (P.R. China)

T. Gao, Y. F. Zhang, Prof. Z. F. Liu
Department of Chemistry, Peking University
Beijing (P.R. China)

[+] These authors contributed equally to this work.

[**] This work was supported by the start-up funding from the HIT and the National Science Foundation of China (21373070, 21173061, 21303030). W.Q.T. thanks the State Key Lab of Urban Water Resource and Environment (HIT) (2014TS01), and the Open Project of State Key Laboratory of Supramolecular Structure and Materials (JLU) (SKLSSM201404) for financial support.

Supporting information for this article is available on the WWW under http://dx.doi.org/10.1002/anie.201400273.

the self-assembly behavior of a series of organic molecules have been studied,[17] to the best of our knowledge this is the first molecular-level investigation of the on-surface condensation reaction on graphene. The properties of graphene are more complex than highly uniform graphite. The different facets, edge states at step edges, kinks, and defects may result in different interactions with graphene, and thus change its electronic properties.[18] How the non-uniformity of the electronic properties of the SLG-copper surface may affect the on-surface condensation is a very interesting point in view of the reaction mechanism. The well-established transfer techniques for graphene[19] also enables the so-prepared surface COF-graphene composite material to be transferred to various substrates.

An extended adlayer of π-conjugated surface $COF_{BTA\text{-}PDA}$ was observed by STM several minutes after applying one droplet of the mixture of the two precursors to the graphene surface (Figure 1a). The surface $COF_{BTA\text{-}PDA}$ extends all over

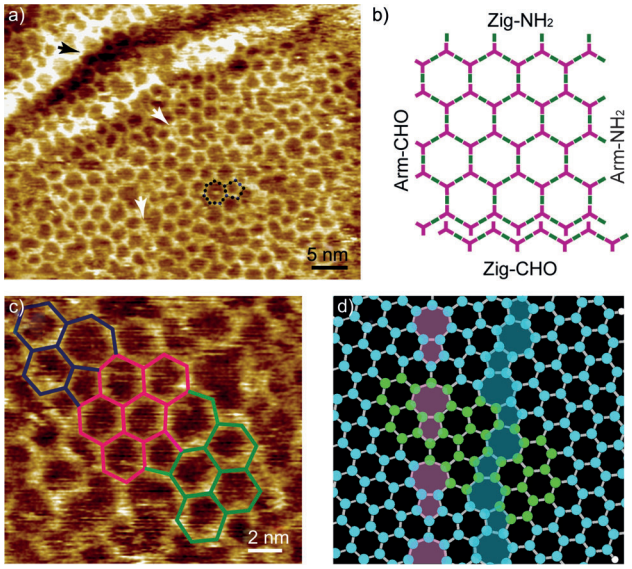

Figure 1. a) STM image of surface $COF_{BTA\text{-}PDA}$ on SLG-copper. A "5 + 7" defect is highlighted by an overlaid schematic model and two typical domain boundaries are marked by the white arrows. A perfect chain of hexagons crossing the step edge of copper is marked by the black arrow. b) A schematic illustration of the different domain boundaries. c) An enlarged STM image of three differently oriented domains with schematic illustrations overlaid. d) A structural model of the LAGB-I and LAGB-II domain boundaries of graphene, with the Stone-Wales defects highlighted with violet and blue. The carbon atoms of a structurally similar patch correspond to the surface $COF_{BTA\text{-}PDA}$ in (c) is highlighted in green. The tunneling conditions were $I_{set} = 700$ pA, $V_{bias} = 10$ mV for a) and c).

the graphene surface and the final structure is unperturbed by steps of the underlying copper foil, as indicated by the black arrow. About 70% of the vertices are triple-coordinated, which indicates the completeness of the Schiff base reaction. The densities of pentagons, hexagons, and heptagons were found to be 0.012, 0.033, and 0.008 nm^{-2}, respectively. The lattice parameters were $a = b = 2.1 \pm 0.1$ nm, $\alpha = 60 \pm 2°$, which is in good agreement with the chemical structure model and DFT simulations ($a = b = 22.23$ Å, $\alpha = 60°$), thus confirming the formation of a covalent bond. Domain boundaries resulting from incomplete reaction were often observed (Figure 1a, white arrows). This indicates that the growth of surface $COF_{BTA\text{-}PDA}$ happens simultaneously at different sites. According to the symmetry of the surface $COF_{BTA\text{-}PDA}$, the domain boundary could be either armchair or zig-zag, terminated with either aldehyde or amine groups, which can be denoted as Arm-NH_2, Arm-CHO, Zig-NH_2, and Zig-CHO, respectively (Figure 1b). However, our observations indicate that the dominant case is Zig-CHO, with the other combinations (Zig-NH_2, Arm-CHO, Arm-NH_2) being very rarely observed (see Figure S3 in the Supporting Information), despite *p*-phenylenediamine being in excess in the solution.

It is very interesting that a typical defect, one heptagon neighboring a pentagon, was often observed in the 2D surface $COF_{BTA\text{-}PDA}$ (Figure 1a), which is similar as the Stone–Wales defect of graphene.[18] These "5 + 7" defects appear frequently when two domains of surface $COF_{BTA\text{-}PDA}$ with different orientations meet (Figure 1c). As measured from the STM image, the angles between the blue and red, and the red and green domains are approximately 37° and 23°, respectively. According to the atomic model proposed by Yazyev and Louie, these two "5 + 7" defects are consistent with LAGB-I and LAGB-II grain boundaries of graphene (Figure 1d).[20] Notably, similar growth defects were also observed on single-layer silica films grown on Ru(0001),[21] thus implying that such defects are common for covalently connected honeycomb systems.

The in situ formation of surface $COF_{BTA-PDA}$ at the liquid/graphene interface can achieve equilibrium within minutes, while dynamic self-healing of the defects can be observed in situ. Figure 2 shows two consecutive STM images recorded

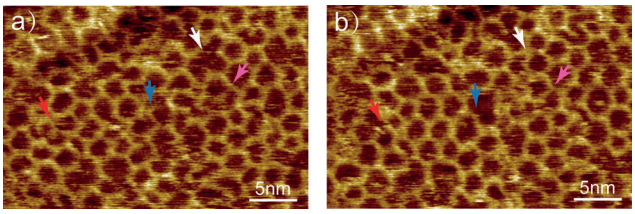

Figure 2. Two successive STM images showing the dynamic process of Schiff-base coupling at the octanoic acid/graphene interface. The time interval is 1.08 min. The arrows highlight the sites where noticeable changes happened. The tunneling conditions were $I_{set} = 700$ pA, $V_{bias} = 10$ mV.

on the same area. The white arrow indicates a large open pore which was patched by formation of a pentagon and a hexagon. There are no precursors or oligomers adsorbed in the pore in the initial stage; they may have come from the supernatant solution. The red, violet, and blue arrows highlight the repairing of the surface $COF_{BTA\text{-}PDA}$ and formation of new covalent bonds between already existing oligomers and surface $COF_{BTA\text{-}PDA}$. The oligomers appear with noticeably lower contrast before it is integrated into the surface COF through formation of a covalent bond. This is either due to

changes in the electronic properties before and after bond formation,[6] or due to a higher mobility of the oligomer. Scanning of the STM tip can also have an effect on the self-healing process. Analysis of the density and percentage of polygons in the same area after continuous scanning reveals that tip scanning, especially with low bias, may partially destroy the surface COF, while the surface COF heals quickly (within two minutes) after the bias back to imaging mode (see Figure S6 in the Supporting Information). The relative abundance of different polygons also shows a trend of equilibrium, which remains nearly constant during the manipulation.

Although the as-prepared CVD-grown single-layer graphene covers the whole surface of the copper foil, different facets and areas exist with different corrugations on the copper substrate.[17,18] Although we have evidence that the surface $COF_{BTA\text{-}PDA}$ covers almost the entire graphene surface, we find that the best contrast appears with different tunneling conditions for different areas. Figure 3 demonstrates how the tunneling conditions influence the appearance of surface $COF_{BTA\text{-}PDA}$. This imaged area can be divided into three parts, in the center the copper underlayer is highly crystalline with big flat terraces, while in the upper and lower parts of the image the copper substrate has more roughness because of the existence of small facets and even amorphous regions. We believe that graphene interacts more strongly with the copper substrate when it rests on flat terraces than over highly corrugated regions. A transition area exists between each section. With relatively high tunneling bias ($I_{set} = 20$ pA, $V_{bias} = 500$ mV, Figure 3a) the whole image has a fuzzy appearance, but surface $COF_{BTA-PDA}$ can be identified as covering the entire surface. By raising the tunneling current to 700 pA and lowering the sample bias to 20 mV (Figure 3c), the surface $COF_{BTA\text{-}PDA}$ on the flat terraces has the best contrast. The above tunneling conditions are normally used to get atomically resolved graphene lattices. However, when covered with surface $COF_{BTA\text{-}PDA}$, it is difficult to get the graphene lattice on the flat terraces, since the surface $COF_{BTA\text{-}PDA}$ always contributes to the imaging contrast (see Figure S4 in the Supporting Information). This indicates that a strong coupling exists between the surface $COF_{BTA\text{-}PDA}$ and graphene in this area. As we slightly increase the tunneling bias and lowering the tunneling current, surface $COF_{BTA\text{-}PDA}$ at the transition areas show higher resolution (Figure 3b). As our DFT calculations indicate significant mixing of states between surface $COF_{BTA\text{-}PDA}$ and graphene, we attributed the above observation to the strong coupling between surface $COF_{BTA\text{-}PDA}$ and graphene, and to spatial variation in the interaction between the surface $COF_{BTA\text{-}PDA}$-graphene and the copper substrate.

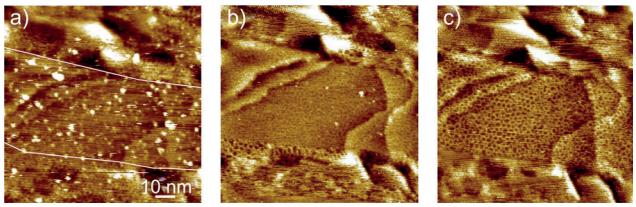

Figure 3. STM images showing the contrast dependence on tunneling conditions. Surface $COF_{BTA\text{-}PDA}$ appears with different contrast on different parts of SLG-copper. The white lines in (a) mark the boundaries of the crystalline terrace. The bright particles observed in (a) are attributed to physisorbed oligomers. a) $I_{set} = 20$ pA, $V_{bias} = 500$ mV; b) $I_{set} = 100$ pA, $V_{bias} = 500$ mV; c) $I_{set} = 700$ pA, $V_{bias} = 20$ mV.

To explore the electronic structure and the interaction between graphene and the surface COF, state-of-the-art electronic structure calculations based on density function theory and the project augmented wave method were performed using the VASP software package.[22] The calculations have been carried out on mono-layer graphene (The addition of Cu-substrate has very slight effect on the structure of surface $COF_{BTA\text{-}PDA}$, see supporting information). As shown in Figure 4, after relaxation graphene and the surface $COF_{BTA\text{-}PDA}$ match well and the graphene stays mostly planar. The bond lengths of C-C, C=C, C-N and C=N in surface $COF_{BTA\text{-}PDA}$ and in surface $COF_{BTA\text{-}PDA}$-graphene complex (denoted as G-surface $COF_{BTA\text{-}PDA}$ here after) are close to each other (see Supporting Information), indicative of small tension in the G-surface $COF_{BTA\text{-}PDA}$. Upon adsorption, the average distance between graphene and the surface $COF_{BTA\text{-}PDA}$, that is, 3.28 Å, falls into the range of van der Waals interaction. The binding energy of surface $COF_{BTA\text{-}PDA}$ to

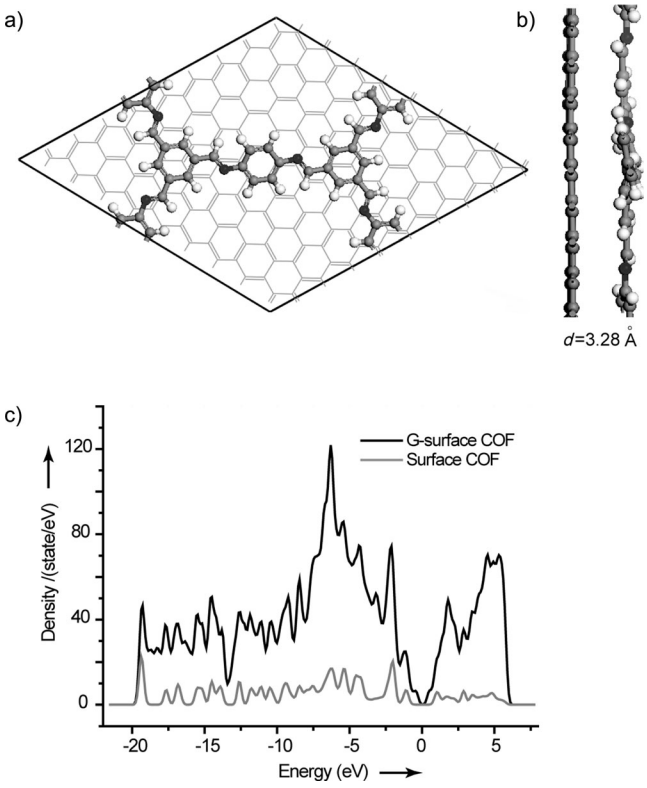

Figure 4. a,b) Geometrical structures of G-surface $COF_{BTA\text{-}PDA}$ in the unit cell (top and side views). c) Density of states of G-surface $COF_{BTA\text{-}PDA}$ and surface $COF_{BTA\text{-}PDA}$ (Fermi level is set at 0 eV).

graphene is −2.41 eV per unit cell, indicative of energetically favored adsorptions.

The density of states (DOS) of the G-surface $COF_{BTA\text{-}PDA}$ and surface $COF_{BTA\text{-}PDA}$ are presented in Figure 4c. Upon adsorption onto graphene, the shape of DOS of the complex near the Fermi level is dominated by graphene and the band gap of the G-surface $COF_{BTA\text{-}PDA}$ complex is very small (0.081 eV). For analyzing the electronic properties of the complex, the band structure and charge distribution of the frontier bands near the Fermi energy of G-surface $COF_{BTA\text{-}PDA}$ are plotted in Figure 5. There are two types of bands in the

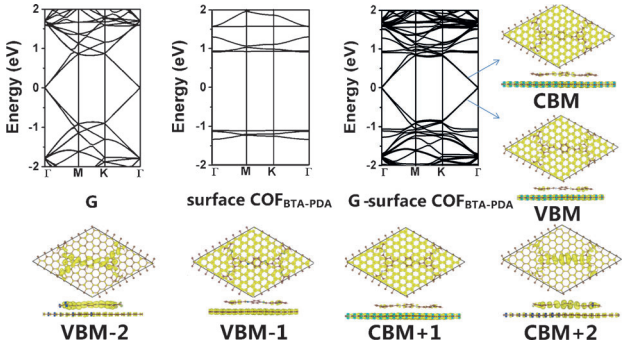

Figure 5. The band structures of graphene, surface $COF_{BTA\text{-}PDA}$, G-surface $COF_{BTA\text{-}PDA}$ and the decomposed charge density of G-surface $COF_{BTA\text{-}PDA}$ near the Fermi level (Fermi level is set at 0 eV).

G-surface $COF_{BTA\text{-}PDA}$: flat bands associated with surface $COF_{BTA\text{-}PDA}$ and dispersive bands from graphene. For comparison, the band structures of the free standing graphene and surface $COF_{BTA\text{-}PDA}$ are also shown. It can be seen that after integration with graphene, the shape of bands associated with surface $COF_{BTA\text{-}PDA}$ also become dispersive due to interaction with graphene. The band structure of surface $COF_{BTA\text{-}PDA}$ shows a band gap around 2 eV, indicating that the free standing Schiff-base surface $COF_{BTA\text{-}PDA}$ is a 2D organic semiconductor. In the valence band maximum (VBM) and the conduction band minimum (CBM), charge density mainly localizes on graphene. Similar charge distribution is observed in the VBM-1 and CBM + 1. In the bands below VBM-1 (e.g. VBM-2) and above CBM + 1 (e.g. CBM + 2), charge density mainly locates on surface $COF_{BTA\text{-}PDA}$, that is, VBM-2 and CBM + 2 are dominantly assigned to the contribution from VBM and CBM of isolated surface $COF_{BTA\text{-}PDA}$ respectively, as shown in Figure 5. However, the contribution from graphene in VBM-2 and CBM + 2 is not negligible (and visa versa), which indicates significant mixing of the electronic states of surface $COF_{BTA\text{-}PDA}$ and graphene. The charge distribution of the frontier valence bands near the Fermi level on the surface $COF_{BTA\text{-}PDA}$ and G-surface $COF_{BTA\text{-}PDA}$ suggests significant electron delocalization, that is, strong two-dimensional π-conjugation in the surface $COF_{BTA\text{-}PDA}$. Thus the imine based surface COFs can be an intriguing two-dimensional organic semiconductor with tunable band gap.

To summarize, we applied a simple while efficient methodology for the preparation of surface $COF_{BTA\text{-}PDA}$ at octanoic acid/graphene interface. The reaction happens preferentially at the solid/liquid interface due to the adsorption of precursors. By controlling the concentration of precursors the reaction can be limited to the interface. STM imaging provides high spatial resolution about the structure of surface $COF_{BTA\text{-}PDA}$. The reaction at the liquid/graphene interface is unperturbed by steps of the underlying substrate. In the STM image, we had observed the "5 + 7" defects which is an analogue of Stone-Wales defect of graphene. A tunneling condition dependence was revealed for the contrast of surface $COF_{BTA\text{-}PDA}$ on different part of graphene surface, which implies that there is a strong coupling between surface $COF_{BTA\text{-}PDA}$ and graphene. This hypothesis has been verified by our DFT calculations. The band structure and distribution of charge density also confirms the conjugated structure of the surface $COF_{BTA\text{-}PDA}$. Both in the free standing surface $COF_{BTA\text{-}PDA}$ and the G-surface $COF_{BTA\text{-}PDA}$ complex the charge density is highly delocalized. This leads to the prospect that the free standing surface $COF_{BTA\text{-}PDA}$ by itself can be an intriguing two-dimensional organic semiconductor, and its band gap can be tuned by alternating the backbone structure or attaching functional groups. The well developed transfer techniques for graphene make it possible to transfer the G-surface $COF_{BTA\text{-}PDA}$ composite to various substrates and to investigate its properties as a true 2D material. Considering the coordination properties of the Schiff-base and the strong coupling between surface $COF_{BTA\text{-}PDA}$ and graphene such composites may also find applications in the field of chemical sensing and heterocatalysis.

Received: January 10, 2014

Keywords: density functional calculations · graphene · Schiff base · STM · surface covalent organic framework

[1] a) A. Thomas, *Angew. Chem.* **2010**, *122*, 8506 – 8523; *Angew. Chem. Int. Ed.* **2010**, *49*, 8328 – 8344; b) X. Feng, X. S. Ding, D. L. Jiang, *Chem. Soc. Rev.* **2012**, *41*, 6010 – 6022.

[2] a) C. J. Doonan, D. J. Tranchemontagne, T. G. Glover, J. R. Hunt, O. M. Yaghi, *Nat. Chem.* **2010**, *2*, 235 – 238; b) N. L. Campbell, R. Clowes, L. K. Ritchie, A. I. Cooper, *Chem. Mater.* **2009**, *21*, 204 – 206; c) H. Furukawa, O. M. Yaghi, *J. Am. Chem. Soc.* **2009**, *131*, 8875 – 8883.

[3] a) Y. G. Zhang, S. N. Riduan, *Chem. Soc. Rev.* **2012**, *41*, 2083 – 2094; b) S. Wan, J. Guo, J. Kim, H. Ihee, D. L. Jiang, *Angew. Chem.* **2009**, *121*, 5547 – 5550; *Angew. Chem. Int. Ed.* **2009**, *48*, 5439 – 5442.

[4] J. Sakamoto, J. van Heijst, O. Lukin, A. D. Schlüter, *Angew. Chem.* **2009**, *121*, 1048 – 1089; *Angew. Chem. Int. Ed.* **2009**, *48*, 1030 – 1069.

[5] a) P. Zhu, V. Meunier, *J. Chem. Phys.* **2012**, *137*, 244703; b) L. Cardenas, R. Gutzler, J. Lipton-Duffin, C. Y. Fu, J. L. Brusso, L. E. Dinca, M. Vondráček, Y. Fagot-Revurat, D. Malterre, F. Rosei, D. F. Perepichka, *Chem. Sci.* **2013**, *4*, 3263 – 3268.

[6] a) Y. G. Zhou, Z. G. Wang, P. Yang, X. T. Zu, F. Gao, *J. Mater. Chem.* **2012**, *22*, 16964 – 16970; b) R. Gutzler, D. F. Perepichka, *J. Am. Chem. Soc.* **2013**, *135*, 16585 – 16594.

[7] I. Berlanga, R. Mas-Ballesté, F. Zamora, *Chem. Commun.* **2012**, *48*, 7976 – 7978.

[8] J. W. Colson, A. R. Woll, A. Mukherjee, M. P. Levendorf, E. L. Spitler, V. B. Shields, M. G. Spencer, J. Park, W. R. Dichtel, *Science* **2011**, *332*, 228 – 231.

[9] a) L. Grill, M. Dyer, L. Lafferentz, M. Persson, M. V. Peters, S. Hecht, *Nat. Nanotechnol.* **2007**, *2*, 687 – 691; b) M. I. Veld, P. Iavicoli, S. Haq, D. B. Amabilino, R. Raval, *Chem. Commun.* **2008**, 1536 – 1538; c) N. A. A. Zwaneveld, R. Pawlak, M. Abel, D. Catalin, D. Gigmes, D. Bertin, L. Porte, *J. Am. Chem. Soc.* **2008**, *130*, 6678 – 6679; d) S. Weigelt, C. Busse, C. Bombis, M. M. Knudsen, K. V. Gothelf, E. Lægsgaard, F. Besenbacher, T. R. Linderoth, *Angew. Chem.* **2008**, *120*, 4478 – 4482; *Angew. Chem. Int. Ed.* **2008**, *47*, 4406 – 4410.

[10] a) M. Bieri, M. T. Nguyen, O. Gröning, J. Cai, M. Treier, K. Ait-Mansour, P. Ruffieux, C. A. Pignedoli, D. Passerone, M. Kastler, K. Müllen, R. Fasel, *J. Am. Chem. Soc.* **2010**, *132*, 16669 – 16676; b) M. O. Blunt, J. C. Russell, N. R. Champness, P. H. Beton, *Chem. Commun.* **2010**, *46*, 7157 – 7159.

[11] D. Y. Zhong, J. H. Franke, S. K. Podiyanachari, T. Blömker, H. M. Zhang, G. Kehr, G. Erker, H. Fuchs, L. F. Chi, *Science* **2011**, *334*, 213 – 216.

[12] a) A. Gourdon, *Angew. Chem.* **2008**, *120*, 7056 – 7059; *Angew. Chem. Int. Ed.* **2008**, *47*, 6950 – 6953; b) M. Lackinger, W. M. Heckl, *J. Phys. D* **2011**, *44*, 464011 – 464024.

[13] J. Greenwood, C. J. Baddeley, *Langmuir* **2013**, *29*, 653 – 657.

[14] a) C. Z. Guan, D. Wang, L. J. Wan, *Chem. Commun.* **2012**, *48*, 2943 – 2945; b) R. Tanoue, R. Higuchi, N. Enoki, Y. Miyasato, S. Uemura, N. Kimizuka, A. Z. Stieg, J. K. Gimzewski, M. Kunitake, *ACS Nano* **2011**, *5*, 3923 – 3929.

[15] J. F. Dienstmaier, D. D. Medina, M. Dogru, P. Knochel, T. Bein, W. M. Heckl, M. Lackinger, *ACS Nano* **2012**, *6*, 7234 – 7242.

[16] a) X. H. Liu, C. Z. Guan, S. Y. Ding, W. Wang, H. J. Yan, D. Wang, L. J. Wan, *J. Am. Chem. Soc.* **2013**, *135*, 10470 – 10475; b) L. R. Xu, X. Zhou, Y. X. Yu, W. Q. Tian, J. Ma, S. B. Lei, *ACS Nano* **2013**, *7*, 8066 – 8073.

[17] a) B. Li, K. Tahara, J. Adisoejoso, W. Vanderlinden, K. S. Mali, S. De Gendt, Y. Tobe, S. De Feyter, *ACS Nano* **2013**, *7*, 10764 – 10772; b) Q. H. Wang, M. C. Hersam, *Nat. Chem.* **2009**, *1*, 206 – 211; c) M. Roos, D. Künzel, B. Uhl, H.-H. Huang, O. B. Alves, H. E. Hoster, A. Gross, R. J. Behm, *J. Am. Chem. Soc.* **2011**, *133*, 9208 – 9211; d) X. L. Sun, J. Zhang, C. Y. Zhang, X. N. Wang, P. A. Hu, Y. B. Mu, X. B. Wan, Z. X. Guo, S. B. Lei, *Chem. Commun.* **2013**, *49*, 10317 – 10319.

[18] a) Y. F. Zhang, T. Gao, Y. B. Gao, S. B. Xie, Q. Q. Ji, H. L. Peng, Z. F. Liu, *ACS Nano* **2011**, *5*, 4014 – 4022; b) F. Banhart, J. Kotakoski, A. V. Krasheninnikov, *ACS Nano* **2011**, *5*, 26 – 41.

[19] S. Bae, H. Kim, Y. Lee, X. F. Xu, J. S. Park, Y. Zheng, J. Balakrishnan, T. Lei, H. R. Kim, Y. Song, Y. J. Kim, K. S. Kim, B. Özyilmaz, J. H. Ahn, B. H. Hong, S. Lijima, *Nat. Nanotechnol.* **2010**, *5*, 574 – 578.

[20] O. V. Yazyev, S. G. Louie, *Phys. Rev. B* **2010**, *81*, 195420.

[21] L. Lichtenstein, C. Büchner, B. Yang, S. Shaikhutdinov, M. Heyde, M. Sierka, R. Włodarczyk, J. Sauer, H. J. Freund, *Angew. Chem.* **2012**, *124*, 416 – 420; *Angew. Chem. Int. Ed.* **2012**, *51*, 404 – 407.

[22] G. Kresse, J. Furthmuller, *Phys. Rev. B* **1996**, *54*, 11169 – 11186.

